Lipoteichoic acid anchor triggers Mincle to drive protective immunity against invasive group A *Streptococcus* infection

Takashi Imai[a,b,c], Takayuki Matsumura[d,1], Sabine Mayer-Lambertz[e,1], Christine A. Wells[f], Eri Ishikawa[b,g], Suzanne K. Butcher[f], Timothy C. Barnett[h,i], Mark J. Walker[h,i], Akihiro Imamura[j], Hideharu Ishida[k,l], Tadayoshi Ikebe[m], Tomofumi Miyamoto[n], Manabu Ato[d], Shouichi Ohga[c], Bernd Lepenies[e], Nina M. van Sorge[o], and Sho Yamasaki[a,b,g,p,2]

[a]Division of Molecular Immunology, Medical Institute of Bioregulation, Kyushu University, 812-8582 Fukuoka, Japan; [b]Department of Molecular Immunology, Research Institute for Microbial Diseases, Osaka University, 565-0871 Osaka, Japan; [c]Department of Pediatrics, Graduate School of Medical Sciences, Kyushu University, 812-8582 Fukuoka, Japan; [d]Department of Immunology, National Institute of Infectious Diseases, 162-8640 Tokyo, Japan; [e]Immunology Unit, Research Center for Emerging Infections and Zoonoses, University of Veterinary Medicine, 30559 Hannover, Germany; [f]The Centre for Stem Cell Systems, Anatomy and Neuroscience, Faculty of Medicine, Dentistry and Health Sciences, University of Melbourne, Melbourne, VIC 3010, Australia; [g]Department of Molecular Immunology, Immunology Frontier Research Center, Osaka University, 565-0871 Osaka, Japan; [h]School of Chemistry and Molecular Biosciences, The University of Queensland, Brisbane, QLD 4072, Australia; [i]Australian Infectious Diseases Research Centre, The University of Queensland, Brisbane, QLD 4072, Australia; [j]Department of Applied Bio-organic Chemistry, Gifu University, 501-1193 Gifu, Japan; [k]Faculty of Applied Biological Sciences, Gifu University, 501-1193 Gifu, Japan; [l]Center for Highly Advanced Integration of Nano and Life Sciences, Gifu University, 501-1193 Gifu, Japan; [m]Department of Bacteriology I, National Institute of Infectious Diseases, 162-8640 Tokyo, Japan; [n]Department of Natural Products Chemistry, Graduate School of Pharmaceutical Sciences, Kyushu University, 812-8582 Fukuoka, Japan; [o]Medical Microbiology, University Medical Center Utrecht, Utrecht University, 3584 CX Utrecht, The Netherlands; and [p]Division of Molecular Immunology, Medical Mycology Research Center, Chiba University, 260-8673 Chiba, Japan

Edited by Lewis L. Lanier, University of California, San Francisco, CA, and approved September 26, 2018 (received for review June 1, 2018)

Group A *Streptococcus* (GAS) is a Gram-positive bacterial pathogen that causes a range of diseases, including fatal invasive infections. However, the mechanisms by which the innate immune system recognizes GAS are not well understood. We herein report that the C-type lectin receptor macrophage inducible C-type lectin (Mincle) recognizes GAS and initiates antibacterial immunity. Gene expression analysis of myeloid cells upon GAS stimulation revealed the contribution of the caspase recruitment domain-containing protein 9 (CARD9) pathway to the antibacterial responses. Among receptors signaling through CARD9, Mincle induced the production of inflammatory cytokines, inducible nitric oxide synthase, and reactive oxygen species upon recognition of the anchor of lipoteichoic acid, monoglucosyldiacylglycerol (MGDG), produced by GAS. Upon GAS infection, Mincle-deficient mice exhibited impaired production of proinflammatory cytokines, severe bacteremia, and rapid lethality. GAS also possesses another Mincle ligand, diglucosyldiacylglycerol; however, this glycolipid interfered with MGDG-induced activation. These results indicate that Mincle plays a central role in protective immunity against acute GAS infection.

innate immunity | bacterial infection | C-type lectin receptors | glycolipids | adjuvant

Group A *Streptococcus* (GAS, *Streptococcus pyogenes*) is a Gram-positive bacterial pathogen that causes various self-limiting diseases, including pharyngitis, impetigo, and scarlet fever. Importantly, GAS also causes severe invasive infections such as streptococcal toxic shock syndrome, necrotizing fasciitis, and bacteremia (1). Recurrent GAS infection increases the risk for GAS-associated autoimmune diseases, such as rheumatic fever and rheumatic heart disease (2). Invasive infections and autoimmune complications are associated with high mortality despite the sensitivity of GAS to antibiotics, including penicillins (3). To control such devastating GAS-mediated disease outcomes, it is crucial to improve our understanding of the mechanism(s) by which the immune system senses GAS and triggers protective responses.

A number of studies have demonstrated that innate immune responses play a predominant role in host protection against GAS (4–6). Neutrophils and myeloid cells are important classes of innate immune cells that fulfill nonredundant roles in preventing GAS dissemination (7, 8). The common TLR adaptor MyD88 substantially contributes to GAS-induced cytokine production (9–11), and MyD88-deficient mice are susceptible to GAS challenge (12). The upstream pattern recognition receptor (PRR) that triggers MyD88-dependent responses has not been clearly elucidated despite the fact that individual TLRs recognize and respond to isolated GAS components in vitro. For example, TLR2 recognizes GAS lipoteichoic acid (LTA), an essential glycerol phosphate polymer with a glycosyldiacylglycerol membrane anchor, to induce myeloid cell activation (13). In addition, mouse TLR13 interacts with bacterial rRNA (14) and is involved in GAS recognition in vitro (15). However, the in vivo role of TLRs is not fully understood, as mice lacking individual TLRs did not show consistent results regarding GAS susceptibility (7, 16, 17). In addition, analysis of GAS-susceptible patients suggests the involvement of MyD88-independent receptor(s) (18).

Significance

Group A *Streptococcus* (GAS) causes invasive streptococcal infections in humans, resulting in high mortality. Thus, GAS is also known as "killer bacteria" or "flesh-eating bacteria." The mechanism by which the immune system recognizes this potent pathogen remains elusive. In this study, we showed that the innate immune receptor Mincle (macrophage inducible C-type lectin) plays pivotal roles against invasive GAS infection through the recognition of monoglucosyldiacylglycerol (MGDG), a component of the lipoteichoic acid anchor. MGDG induced proinflammatory cytokines, ROS, and NO production in a Mincle-dependent manner. In an invasive GAS infection model, Mincle-deficient mice exhibited severe bacteremia and rapid lethality. These results indicate that Mincle plays a central role in protective immunity against acute GAS infection.

Author contributions: T. Imai, T. Matsumura, M.A., B.L., N.M.v.S., and S.Y. designed research; T. Imai, T. Matsumura, S.M.-L., E.I., S.K.B., T.C.B., T. Miyamoto, and N.M.v.S. performed research; C.A.W., M.J.W., A.I., H.I., T. Ikebe, and S.O. contributed new reagents/analytic tools; T. Imai, T. Matsumura, C.A.W., M.J.W., T. Miyamoto, M.A., B.L., and N.M.v.S. analyzed data; and T. Imai, T. Miyamoto, N.M.v.S., and S.Y. wrote the paper.

The authors declare no conflict of interest.

This article is a PNAS Direct Submission.

Published under the PNAS license.

[1]T. Matsumura and S.M.-L. contributed equally to this work.

[2]To whom correspondence should be addressed. Email: yamasaki@biken.osaka-u.ac.jp.

This article contains supporting information online at www.pnas.org/lookup/suppl/doi:10.1073/pnas.1809100115/-/DCSupplemental.

Indeed, several PRRs other than TLRs are involved in immune responses to GAS, including the Nod-like receptor NLRP3 (11, 19). However, NLRP3-deficient mice are still capable of eliminating GAS (11).

Recently, an additional family of PRRs, termed C-type lectin receptors (CLRs), was defined as receptors that recognize glycosylated pathogen-associated molecular patterns (PAMPs) (20, 21). Myeloid cells express many CLRs that activate inflammatory responses through an immunoreceptor tyrosine-based activation motif (ITAM) located in their own cytoplasmic tails, or by coupling with ITAM-bearing signaling subunits (22). In either case, the ITAM undergoes phosphorylation upon ligand engagement and recruits tyrosine kinase Syk to activate the pivotal adaptor complex CARD9-Bcl10-Malt1. This signaling cascade triggers multiple innate responses, including the production of inflammatory mediators and up-regulation of costimulatory molecules (23, 24). Among the ITAM-coupled CLRs, we previously reported that macrophage inducible C-type lectin (Mincle), MCL, Dectin-2, and DCAR are FcRγ-coupled receptors that preferentially recognize glycolipids from pathogens (25–29). In particular, Mincle recognizes diverse glycolipids such as mycobacterial trehalose dimycolate (TDM) (25), pneumococcal glucosyl diacylglycerol (30), and other glucose- or mannose-containing glycolipids (31). Based on the importance of myeloid cells in GAS immune defense, and the fact that no previous studies have probed the role of CLRs in GAS recognition in host defense, we hypothesized that a specific CLR may recognize GAS through glycolipid ligand(s) to initiate immune responses.

In the present study, we show that the C-type lectin Mincle recognizes GAS through the LTA anchor glycolipid monoglucosyldiacylglycerol (MGDG) of GAS to initiate cytokine and reactive oxygen species (ROS) production. We further demonstrate, using Mincle-deficient mice, that this innate immune pathway plays a pivotal role in protective immunity against invasive GAS infection. Finally, GAS also produces a glycolipid that blocks MGDG-induced Mincle activation.

Results

Monocytes Display a CARD9 Signature upon Exposure to GAS. To explore the signaling pathway(s) involved in immune responses against GAS, we carried out capped analysis of gene expression (CAGE) (32, 33). Primary human monocytes were stimulated with human bacterial or fungal pathogens including GAS, *Candida albicans*, *Salmonella typhimurium*, and lipopolysaccharide (LPS). We identified a diverse set of proximal promoters that were induced in response to these stimuli (*SI Appendix*, Fig. S1*A* and Dataset S1). Application of principal component analysis to the dataset highlighted that the transcriptional profile induced by GAS largely overlapped with the profile of *C. albicans* (Fig. 1*A*), for which the involvement of CLR–CARD9 signaling is well established (34–36).

CARD9 Is Required for the Production of Proinflammatory Cytokines in Response to GAS. To validate the observation that CARD9 signaling is involved in the induction of inflammatory responses to GAS infection, we performed in vitro experiments with bone marrow-derived dendritic cells (BMDCs) from WT and CARD9$^{-/-}$ mice. Infection of CARD9$^{-/-}$ BMDCs with GAS demonstrated significantly lower production of TNF and MIP-2 compared with WT (Fig. 1 *B* and *C*).

To identify the molecular triggers for these inflammatory cytokines and chemokines, we extracted hydrophilic and hydrophobic components from GAS using a $CHCl_3$:MeOH:H_2O (C:M:W) solvent and evaluated each extract for its ability to stimulate BMDCs. Only the hydrophobic C:M extract induced the production of TNF in WT BMDCs, which was decreased in CARD9$^{-/-}$ BMDCs (Fig. 1*D*). These results suggest that a component in the lipophilic fraction from GAS is recognized by an innate immune receptor(s) that initiates CARD9-dependent signaling upon GAS infection.

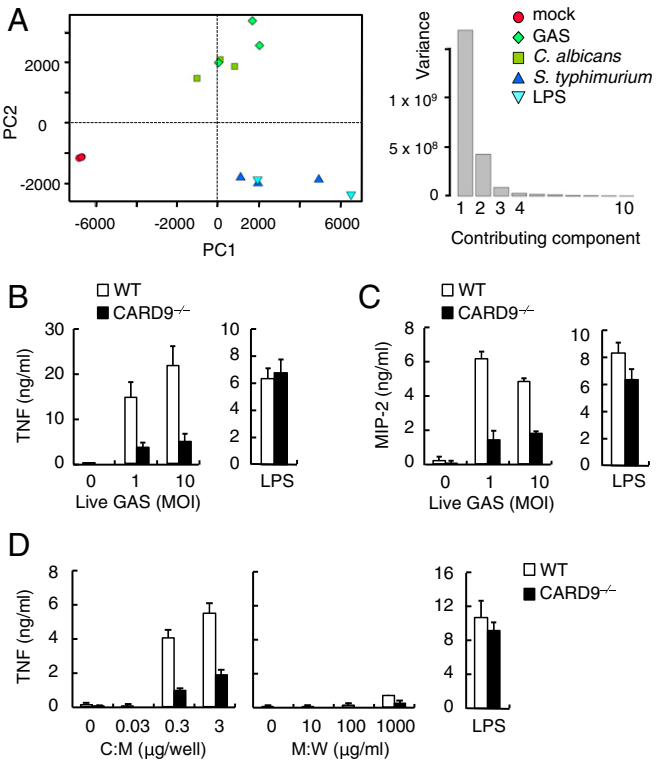

Fig. 1. GAS infection of human monocytes activates CARD9 signaling. (*A*) Principal component (PC) analysis on data from CAGE experiments (*Left*). Primary monocytes from three donors were stimulated with the following for 2 h: GAS, *C. albicans*, *S. typhimurium*, LPS, mock-treated. Data were represented as 2D plot (PC1 vs. PC2), as scree plot indicates major contribution of the first two components to variance in the CAGE data (*Right*). Symbols shown in the same color (green or blue) indicate the same cluster. (*B* and *C*) BMDCs from WT or CARD9$^{-/-}$ mice were infected with GAS (MOI = 1 and 10) or left uninfected. LPS was used as a positive control. At 16 h after infection, the supernatants were collected, and the concentrations of (*B*) TNF and (*C*) MIP-2 were determined by ELISA. (*D*) BMDCs from WT or CARD9$^{-/-}$ mice were stimulated with indicated concentrations of plate-coated lipophilic fraction (C:M) or hydrophilic fraction (M:W) of GAS for 48 h. Supernatants were collected, and the concentration of TNF was determined by ELISA. C:M, chloroform:methanol; M:W, methanol:water. In *B*–*D*, data are presented as mean ± SD and are representative of three independent experiments with similar results.

Mincle Is the CLR That Recognizes the Lipophilic Component from GAS. We next sought to identify the innate immune receptor(s) upstream of CARD9 that recognizes a component in the lipophilic fraction from GAS. We utilized cells expressing NFAT-GFP reporters and a range of innate immune receptors (37). Among the assessed PRRs, cells bearing the CLR Mincle showed high GFP reporter expression in response to the hydrophobic extract from GAS (Fig. 2*A*). This ability was highly conserved across species, as Mincle orthologs derived from mouse, rat, guinea pig, and human all retained activity in this assay (Fig. 2*A*). In addition, the reporter cells expressing mouse Mincle reacted to this fraction in a dose-dependent manner (Fig. 2*B*), allowing the use of Mincle-deficient BMDCs to further examine the contribution of endogenously expressed Mincle to immune signaling. Induction of TNF production by the C:M fraction was decreased in Mincle$^{-/-}$ cells to an extent similar to that observed in CARD9$^{-/-}$ cells (Fig. 2*C*). Consistent with this observation, a Mincle-Ig fusion protein directly bound to GAS (Fig. 2*D*). Furthermore, upon in vitro infection of BMDCs with GAS, TNF production was significantly lower in Mincle$^{-/-}$ BMDCs compared with WT cells (Fig. 2*E*). The contribution of Mincle to BMDC cytokine responses was observed with several GAS isolates (*SI Appendix*, Fig. S2). Correspondingly, evaluation

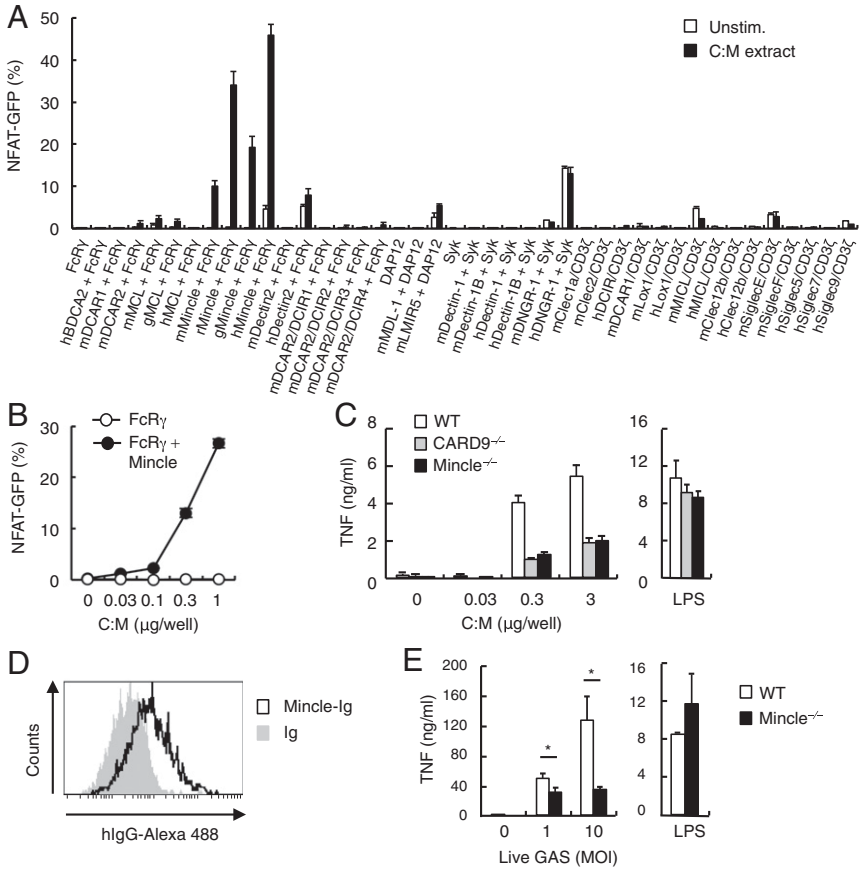

Fig. 2. Mincle recognizes the lipophilic fraction of GAS. (*A*) NFAT-GFP reporter cells expressing various PRRs were left unstimulated or stimulated by plate-coated lipophilic fraction from GAS for 16 h. Induction of GFP was analyzed by flow cytometry, and percent positive cells are plotted. (*B*) The lipophilic fraction (C:M) was plate-coated to stimulate NFAT-GFP reporter cells expressing FcRγ only or mouse Mincle + FcRγ. (*C*) BMDCs from WT, CARD9$^{-/-}$, or Mincle$^{-/-}$ mice were stimulated with the indicated concentrations of plate-coated lipophilic fraction for 16 h. The concentration of TNF was determined by ELISA. (*D*) Live GAS were incubated with human IgG1-Fc (Ig) or Mincle-Ig fusion protein (Mincle-Ig) (1 μg/mL) for 1 h at 4 °C. Bound proteins were detected with anti−hIgG-Alexa 488 by flow cytometry. (*E*) BMDCs from WT or Mincle$^{-/-}$ mice were infected with live GAS (MOI = 1 and 10) or exposed to LPS (10 ng/mL) for 16 h. The concentrations of TNF produced were determined by ELISA. *$P < 0.05$. Data are presented as mean ± SD and are representative of (*A*) two or (*B*–*E*) three independent experiments with similar results.

of the initial CAGE experiment similarly highlights the involvement of Mincle pathway in response to GAS (*SI Appendix*, Fig. S1 *B* and *C*).

These results suggest that Mincle is a major receptor for GAS acting upstream of the CARD9 signaling pathway.

Identification of MGDG as a Mincle Ligand. To identify the GAS-derived Mincle ligand, we separated the C:M fraction of GAS into 16 subfractions by high-performance TLC (HPTLC) followed by copper acetate staining. Each subfraction was assessed for stimulation of the Mincle reporter cells. Spot **1** (subfraction #12) possessed potent ligand activity in Mincle-expressing reporter cells, whereas the most abundant Spot **2** (subfractions #8 and #9) did not have substantial activity (Fig. 3*A*). Purified Spot **1** could be detected as a single spot upon staining with either copper acetate or orcinol, which visualizes organic molecules and sugar moieties, respectively. However, it was not visible after molybdenum blue staining, suggesting that Spot **1** represents a glycolipid lacking phosphate moieties (Fig. 3*B*). Spot **1** activated Mincle-expressing reporter cells in a dose-dependent manner, and its specific activity per milligram of lipid was increased (Fig. 3*C*) compared with that of crude C:M extract (Fig. 2*B*). Furthermore, Mincle-Ig fusion protein directly bound to purified Spot **1** (Fig. 3*D*), further demonstrating that Spot **1** derived from GAS contains a Mincle ligand.

To determine the chemical structure of the compound present in Spot **1**, we used NMR and mass spectrometry (MS) analysis. The ^{1}H-NMR and ^{13}C-NMR spectra of Spot **1** showed proton signals characteristic of α-glucopyranose, glycerol, and unsaturated fatty acid (Fig. 4*A* and *SI Appendix*, Fig. S3*A*). High-resolution electrospray ionization time-of-flight MS (ESI-TOF-MS) analysis of Spot **1** showed molecular-related ion peaks at *m/z* 749.5191, 751.5336, 777.5495, and 779.5656 (Fig. 4*B*). We also determined the fatty acid composition by gas chromatography MS (GC-MS) analysis following methanolysis (*SI Appendix*, Fig. S3*B*). The GC-MS chromatogram of fatty acid methyl esters (FAMEs) showed the major fatty acids of Spot **1** are C16:0, C16:1, C18:1, and C18:0 (Fig. 4*B* and *SI Appendix*, Fig. S3*B*). $RuCl_3/NaIO_4$ oxidation followed by GC-MS analysis revealed the positions of C16:1 and C18:1 double bonds as C11 and C12 (*SI Appendix*, Fig. S3*C*). The combined NMR, ESI-TOF-MS, and GC-MS analyses identify the major component of Spot **1** as MGDG (16:0/18:1) (Fig. 4*C*).

Spot **1**, hereafter referred to as MGDG, bound to the Mincle-Ig protein as did the known ligand, TDM (Fig. 4*D*) (25), and the structure of MGDG fulfills the minimum criteria of Mincle ligand: a polar head consisting of glucose or mannose and a hydrophobic chain (38, 39). MGDG was also recognized by human Mincle in reporter cells and myeloid cells (*SI Appendix*, Fig. S3 *D* and *E*). Thus, we conclude that the Mincle ligand in GAS is MGDG. MGDG constitutes an anchor moiety of the TLR2 ligand membrane-anchored glycopolymer LTA; however, MGDG did not activate NF-κB reporter cells via TLR2 (Fig. 4*E*), and, conversely, Mincle was not activated by intact LTA (Fig. 4*F*).

MGDG Activates Dendritic Cells Through Mincle. We next examined the role of Mincle in MGDG-induced innate immune responses. MGDG stimulated BMDCs to produce proinflammatory cytokines and chemokines, such as TNF, MIP-2, and IL-6, which were completely suppressed in Mincle-deficient cells (Fig. 5 *A*–*C*). Nitric oxide (NO) and ROS are additional potent effectors that are involved in the bactericidal action of myeloid cells (40–42). MGDG also induced the expression of NO synthase 2 (NOS2/iNOS), an NO-producing enzyme, and ROS production in a Mincle-dependent manner (Fig. 5 *D* and *E*), consistent with the finding that the CARD9 pathway induces ROS (24). Importantly, the induction of iNOS and ROS upon infection with live GAS was also impaired in the absence of Mincle (*SI Appendix*, Fig. S4).

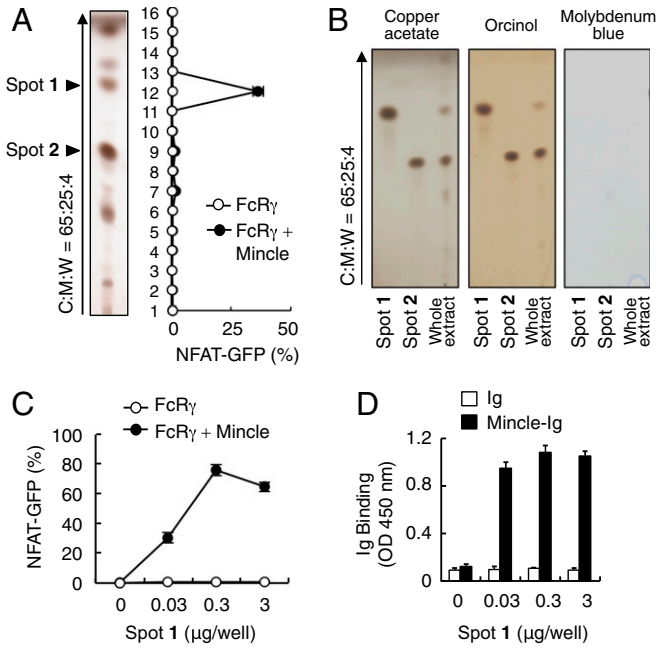

Fig. 3. A GAS glycolipid activates Mincle. (*A*) The lipophilic fraction of GAS was analyzed by HPTLC using C:M:W (65:25:4; vol/vol/vol), stained with copper acetate reagent, and divided into 16 subfractions (*Left*). Each subfraction was coated onto a plate to stimulate reporter cells. Induction of NFAT-GFP was analyzed by flow cytometry (*Right*). (*B*) The C:M extract was analyzed by HPTLC using C:M:W (65:25:4; vol/vol/vol). The HPTLC plates were stained with copper acetate (*Left*), orcinol (*Middle*), or molybdenum blue (*Right*) reagent. (*C*) Reporter cells expressing FcRγ only or Mincle + FcRγ were stimulated with the indicated concentrations of plate-coated purified Spot **1** for 16 h. Induction of NFAT-GFP was analyzed by flow cytometry. (*D*) Ig or Mincle-Ig was incubated with the indicated concentrations of plate-coated purified Spot **1**. Bound proteins were detected with anti–hIgG-HRP. Data are presented as mean ± SD and are representative of three independent experiments with similar results.

Since MGDG had such a pronounced Mincle-dependent effect on BMDC cytokine production, we additionally investigated the downstream consequences for T-cell activation. First, we observed that stimulation of WT BMDCs with MGDG up-regulated the expression of costimulatory molecules, such as CD40, CD80, and CD86 (Fig. 5*F*, *Upper*), which was abolished in the absence of Mincle (Fig. 5*F*, *Lower*). Second, BMDCs were pulsed with the ovalbumin (OVA) antigen peptide and cocultured with T cells from OVA-specific OT-II TCR transgenic mice in the presence or absence of MGDG. Antigen-specific secretion of IL-17 by $CD4^+$ OT-II T cells was significantly augmented when the cells were cocultured with MGDG-treated WT BMDCs. However, this effect was eliminated if the MGDG-treated BMDCs were $Mincle^{-/-}$ (Fig. 5*G*). The effect of MGDG treatment on antigen-dependent IFNγ production was less potent, compared with TDM treatment (Fig. 5*H*). Collectively, these in vitro results suggest that MGDG enhances antigen-presenting cell functions to promote potent Th17 response in a Mincle-dependent manner.

Diglucosyldiacylglycerol Inhibits MGDG-Induced Activation. Given the significant role of Mincle in immunity against GAS, it is possible that GAS may target Mincle for immune evasion. The increase in specific activity during the course of MGDG purification suggested the presence of an inhibiting molecule in the crude lipid fraction of GAS. Indeed, although Spot **2**, the most abundant spot, did not activate Mincle reporter cells (Fig. 3*A* and Fig. 6*A*, *Left*) or BMDCs (Fig. 6*B*, *Left*), it prevented Mincle-mediated activation induced by MGDG (Fig. 6 *A* and *B*, *Right*) and TDM (*SI Appendix*, Fig. S5). In contrast, TLR4-mediated or Dectin-2–mediated BMDC activation were not affected by Spot **2** (Fig. 6C), suggesting that this spot inhibits Mincle-mediated cell activation. Spot **2** also down-regulated the expression of costimulatory molecules in BMDCs induced by MGDG (Fig. 6*D*) or TDM (Fig. 6*E*), and suppressed T-cell activation triggered by MGDG-stimulated BMDCs (Fig. 6*F*). Mincle-Ig protein directly bound Spot **2**, although the binding appeared weaker compared with that of MGDG and TDM (Figs. 4*D* and 6*G* and *SI Appendix*, Fig. S6).

Using NMR and MS, we determined the chemical structure of Spot **2** to be diglucosyldiacylglycerol (DGDG) (mainly 16:1/18:1; 16:0/18:1) (Fig. 7 *A*–*F*). Similar to MGDG, DGDG is produced as an LTA anchor molecule of GAS (43, 44). Indeed, synthetic DGDG suppressed the activation of reporter cells and BMDCs stimulated with MGDG (Fig. 7 *G* and *H*). These results suggest that, although DGDG binds Mincle, it lacks agonistic activity. MGDG and DGDG were detected in the invasive M1 serotype strains 5448 and NIH44, and the M3 serotype strain NIH34, in addition to the noninvasive M1 serotype strains SF370 and Se235, and the M3 serotype strain K33, suggesting that these are shared immunomodulators across different GAS serotypes. Interestingly, DGDG/MGDG ratio varied among the tested strains, which may partly contribute to the different pathogenicity of GAS strains (*SI Appendix*, Figs. S7 *A*–*C* and S8).

Mincle Is Critical for Controlling GAS Infection. Finally, we examined the effect of Mincle on GAS infection in vivo. To gain insight into early responses, WT and $Mincle^{-/-}$ mice were infected intraperitoneally with the invasive GAS strain NIH34. Upon infection, early induction of serum inflammatory cytokines and chemokines, such as IP-10, IL-6, and CXCL1, was significantly suppressed in $Mincle^{-/-}$ mice compared with WT mice (Fig. 8*A*). Regarding the susceptibility to GAS, $Mincle^{-/-}$ mice demonstrated a dramatic increase in mortality compared with WT mice (Fig. 8*B*). Consistent with these results, $Mincle^{-/-}$ mice exhibited severe GAS bacteremia (Fig. 8*C*) and abscess formation in the kidneys, which was not detected in WT mice (Fig. 8 *D* and *E*). Within the abscesses, GAS bacteria were identified as chains of cocci, by staining with hematoxylin (Fig. 8*F*). $Mincle^{-/-}$ mice also suffered exacerbated liver damage, as the degree of hepatocellular vacuolation was higher in $Mincle^{-/-}$ mice than WT mice (Fig. 8 *G* and *H*). Furthermore, $Mincle^{-/-}$ mice developed hypercytokinemia when bacteremia was observed (*SI Appendix*, Fig. S7*D*), suggesting that the rapid increase of bacterial number in mice lacking Mincle-mediated early immune responses eventually causes septic shock and multiple organ failure. Importantly, the role of Mincle in initial cytokine responses and reduced mortality to GAS infection was confirmed by using other GAS strains (*SI Appendix*, Figs. S7*E* and S8). Taken together, these results suggest that Mincle is crucial for protection against early GAS infection.

Discussion

In this manuscript, we have demonstrated that Mincle plays a central role in protective immunity against lethal GAS infection. However, GAS can counteract this protective response by production of DGDG.

Previous studies have reported several innate immune receptors that are involved in GAS sensing and signaling, most notably those receptors that signal through the MyD88-dependent pathway (10–12, 16). However, the roles of individual TLRs in GAS recognition were mainly characterized in vitro, whereas the in vivo susceptibility to GAS infection of mice lacking individual receptors is not clear (7, 16, 17). Strikingly, we show that Mincle deficiency resulted in impaired immune responses and increased susceptibility to GAS infection both in vitro and in vivo. Given that Mincle expression is robustly up-regulated by various stimuli in a MyD88-dependent manner (45, 46), MyD88 pathways may potentially contribute to protective immunity through the induction of Mincle expression. In line with this idea, future experiments may investigate whether introduction of a Mincle transgene into MyD88-deficient mice restores GAS resistance.

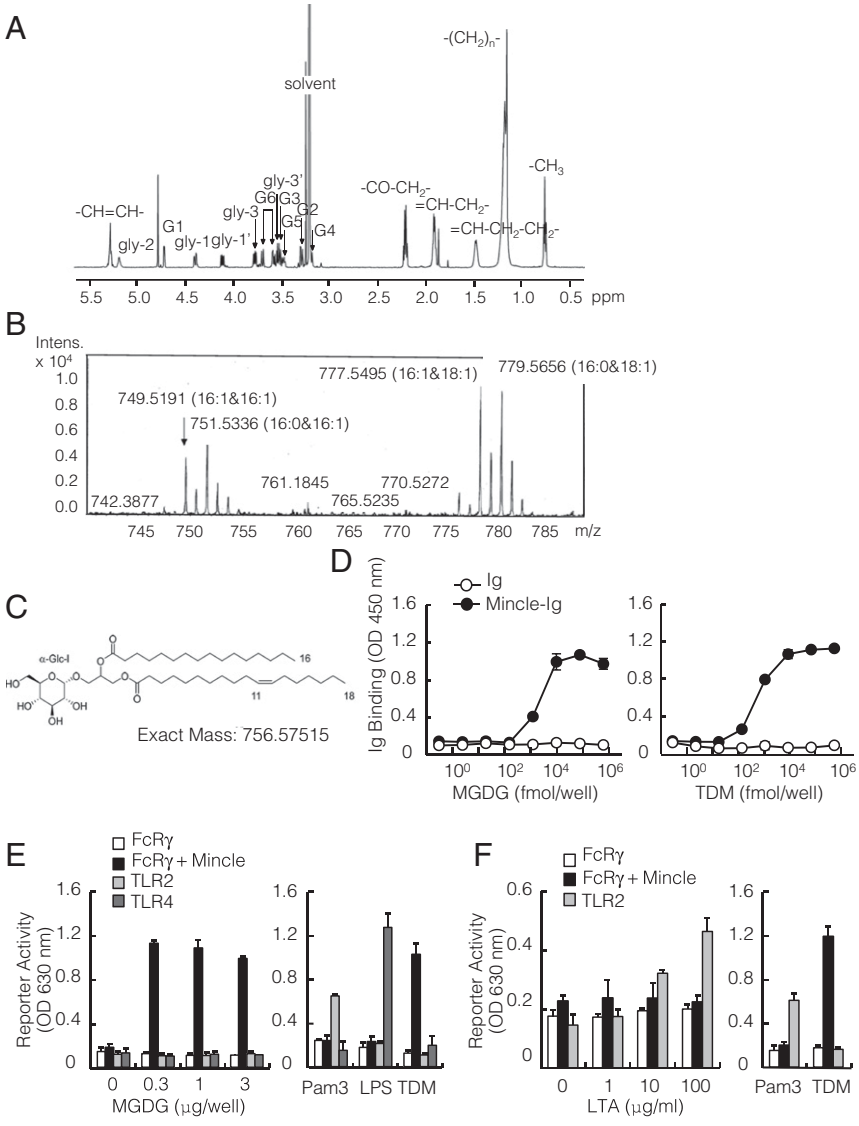

Fig. 4. Identification of MGDG as a Mincle ligand. The (*A*) ^{1}H-NMR spectrum and (*B*) ESI-TOF-MS spectrum of purified Spot **1**. ESI-TOF-MS data of MGDG: *m/z* = 749.5191 $[M+Na]^+$ (calculated for $C_{41}H_{74}NaO_{10}$ Δmmu = −1.7), 751.5336 $[M+Na]^+$ (calculated for $C_{41}H_{76}NaO_{10}$ Δmmu = −0.5), 777.5495 $[M+Na]^+$ (calculated for $C_{43}H_{78}NaO_{10}$ Δmmu = −0.8), and 779.5656 $[M+Na]^+$ (calculated for $C_{43}H_{80}NaO_{10}$ Δmmu = +1.2). (*C*) Chemical structure of MGDG (Spot **1**) from GAS. The Z geometry of the double bond in the fatty acid (FA) side chain was determined by allylic carbon chemical shift at δ_C 28.2, which was assigned by HMBC experiments. (*D*) Ig or Mincle-Ig were incubated with the indicated concentrations of plate-coated TDM or purified MGDG. Bound proteins were detected with anti–hIgG-HRP. (*E*) HEK293 cells expressing FcRγ only, Mincle + FcRγ, TLR2, or TLR4 were stimulated with the indicated concentrations of plate-coated purified MGDG (Spot **1**) for 16 h. Pam3, LPS, and TDM were used as positive controls. Activation of NF-κB was measured by SEAP activity in the supernatants. (*F*) HEK293 cells expressing FcRγ only, Mincle + FcRγ or TLR2 were stimulated with the indicated concentrations of LTA from GAS for 16 h. Pam3 and TDM were used as positive controls. Activation of NF-κB was measured by SEAP activity in the supernatants. Data are presented as mean ± SD and are representative of (*F*) two or (*D* and *E*) three independent experiments with similar results.

Recent reports have highlighted a critical role of the NLRP3 inflammasome and IL-1β in protective immunity against GAS (47–49). Downstream signaling of CLR, including Dectin-1 and Mincle, can directly activate NLRP3 (50, 51). Therefore, GAS-induced inflammasome activation may be partly mediated by the MGDG–Mincle axis in conjunction with the previously reported effector proteins, such as M protein or streptolysin O (11, 19).

GAS infection induces the production of various proinflammatory cytokines, including TNF from myeloid cells (42), which are critical factors in controlling the dissemination of GAS (7). The increased susceptibility of Mincle-deficient mice to early GAS infection is likely due to their reduced ability to produce these key cytokines. NO and ROS are also direct effectors that enhance the elimination of GAS early in infection (41, 42). The Mincle-dependent activation of these pathways may thus synergistically contribute to suppressing the GAS infection process.

Mincle is expressed in a wide range of hematopoietic cells (52–55), and multiple immune cells contribute to immune protection against GAS (5, 8, 56). It is therefore critical to clarify which Mincle-expressing cells are the main contributors to protection against GAS. A recent report showed that, in the early stage of GAS infection, an IFNγ-producing $Gr1^+CD11b^+$ myeloid subset rapidly appears in the periphery and plays a protective role, whereas the receptor that triggers IFNγ production remains unidentified (57). As Mincle is an inducible protein that signals through ITAMs and as ITAM-coupled receptors trigger IFNγ production in lymphocytes, it is plausible that Mincle might also contribute to the robust IFNγ production in this myeloid subset upon sensing GAS-derived MGDG.

We identified two Mincle ligands in the GAS lipophilic fraction: MGDG, which has agonistic activity, and DGDG, which interacts with Mincle but does not initiate signaling. Interestingly, both molecules are membrane anchors for LTA, a common structural feature of the Gram-positive cell envelope (43, 44). As such, glycosyldiacylglycerol is also present in other pathogens (58), and Mincle may play a role in response to such targets. Determination of these immunomodulatory glycolipids together with the expression analysis of the synthase candidates in various microorganisms may help to predict their immunological properties.

The precise role of DGDG in streptococci has been elusive. Disruption of the glucosyltransferase in group B *Streptococcus* (GBS), Δ*iagA* (*invasion-associated gene A*), impaired the invasive capacity in mice, which pointed to a requirement for DGDG in promoting invasion of GBS in host endothelial cells (59). Although no studies have examined DGDG function in GAS, our study herein proposes an action of DGDG as a suppressor of Mincle-mediated responses. The molecular mechanism(s) of this suppression is unknown; however, as DGDG does not suppress the

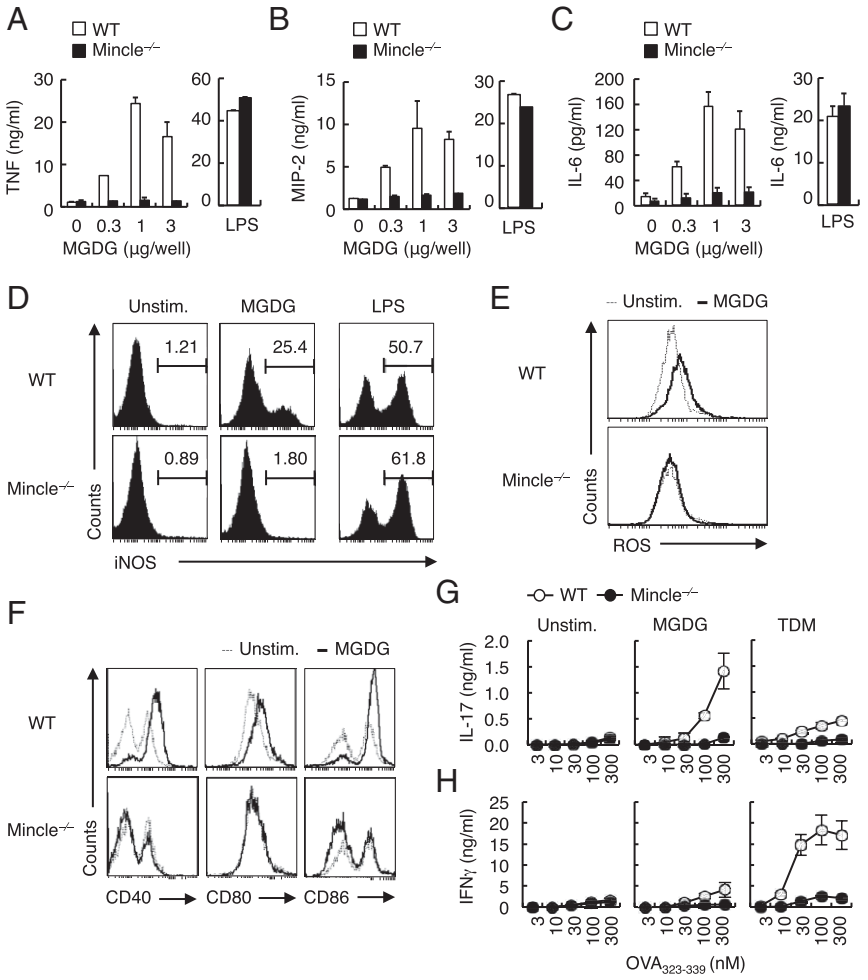

Fig. 5. MGDG induces innate immune responses in a Mincle-dependent manner. (*A*–*C*) BMDCs from WT or Mincle$^{-/-}$ mice were stimulated with the indicated concentrations of plate-coated purified MGDG or LPS for 48 h. The concentrations of (*A*) TNF, (*B*) MIP-2, and (*C*) IL-6 were determined by ELISA. (*D*) BMDCs from WT or Mincle$^{-/-}$ mice were stimulated with plate-coated purified MGDG (10 μg per well) or LPS (10 ng/mL) for 24 h. Intracellular iNOS staining was measured by flow cytometry. (*E*) BMDCs from WT or Mincle$^{-/-}$ mice were left unstimulated (dotted line) or stimulated with plate-coated purified MGDG (10 μg per well; solid line) for 24 h. ROS production was monitored using H_2DCFDA staining followed by FACS analysis. (*F*) BMDCs from WT (*Upper*) or Mincle$^{-/-}$ (*Lower*) mice were left unstimulated (dotted line) or stimulated with plate-coated purified MGDG (3 μg per well; solid line) for 48 h. The surface expressions of CD40, CD80, and CD86 were analyzed by flow cytometry. (*G* and *H*) BMDCs from WT (open circle) or Mincle$^{-/-}$ (closed circle) mice were pulsed with $OVA_{323–339}$ peptide and cocultured with CD4$^+$ OT-II T cells for 4 d in the presence of plate-coated purified MGDG (3 μg per well) or TDM (30 ng per well). The concentrations of IL-17 and IFNγ secreted into the supernatant were determined by ELISA. Data are presented as mean ± SD and are representative of three independent experiments with similar results.

signaling of other PRRs (Fig. 6*C*), it is unlikely that DGDG delivers intrinsic inhibitory signals. Rather, DGDG seems to interfere with the interaction of agonistic ligands to Mincle. For example, some low-affinity/-valency CLR ligands act antagonistically, as exemplified by Dectin-1 ligands (37, 60, 61). Alternatively, as DGDG possesses an α-1,2-linked glucose instead of an α-1,1-linked glucose as found in TDM, it is possible to speculate that the second glucose in DGDG interacts with Mincle in a different way, which may lead to the inefficient receptor clustering. It would be intriguing to speculate that bacteria may regulate the composition of their LTA anchor to escape immune triggering of Mincle. In this respect, it is important that the relative content of MGDG and DGDG in clinical GAS isolates in various stages of infection and diseases be investigated, although virulence is determined by multiple factors. The blockade of DGDG-synthesizing enzyme might provide a therapeutic option by increasing Mincle sensitivity to invasive GAS.

An important unsolved question is how and where Mincle interacts with MGDG/DGDG expressed by GAS. Given that diacylglycerols act as membrane anchors for LTA, it is thought that these glycolipids are localized in the plasma membrane, which lies beneath the thick peptidoglycan layer (43). However, our finding that Mincle-Ig can interact with intact GAS raises the possibility that MGDG/DGDG may be exposed on the cell surface. Additionally, Mincle may recognize degraded moieties of LTA that are shed from or exposed on streptococci (59, 62). Indeed, we could detect MGDG and LTA activity in the GAS culture supernatant (*SI Appendix*, Fig. S9).

In addition to the protective innate immune responses via Mincle in acute GAS infection, Mincle may also promote acquired immune responses during recurrent infection. GAS infection typically induces a Th17 response, which leads to the establishment of protective acquired immunity against GAS in the later phase (63–65). As Mincle ligands potently promote Th17 responses (Fig. 5*G*) (66, 67), which are inhibited by DGDG, the use of a component GAS vaccine retaining MGDG and less DGDG may induce protective immunity against both invasive and recurrent GAS infections. Indeed, in a mouse model, vaccination with liposomes bearing Mincle ligands successfully controlled infections after GAS challenge (68). Hence, GAS-derived MGDG and its derivatives may represent attractive adjuvants for preventing invasive infection and diseases associated with recurrent infection (2, 69, 70).

Materials and Methods

Mice. Mincle-deficient mice (53) were backcrossed for at least nine generations with C57BL/6 mice. CARD9-deficient mice were provided by H. Hara, Kagoshima University, Kagoshima, Japan (23). OVA-specific TCR OT-II transgenic mice were used on a C57BL/6 background. C57BL/6 mice were obtained from Japan Clea or Kyudo. All mice were maintained in a filtered-air laminar-flow enclosure and given standard laboratory food and water ad libitum. Animal protocols were approved by the committee of Ethics on Animal Experiment, Faculty of Medical Sciences, Kyushu University and Research Institute for Microbial Diseases, Osaka University. All work in GAS infection performed using mice was carried out in accordance with the guidelines for animal care approved by the National Institute of Infectious Diseases.

Bacterial Strains. GAS strains used in this study were SF370 (ATCC 700294; American Type Culture Collection), 5448, NIH44, and Se235 of the M1 serotype, and NIH34 and K33 of the M3 serotype. The NIH44, Se235,

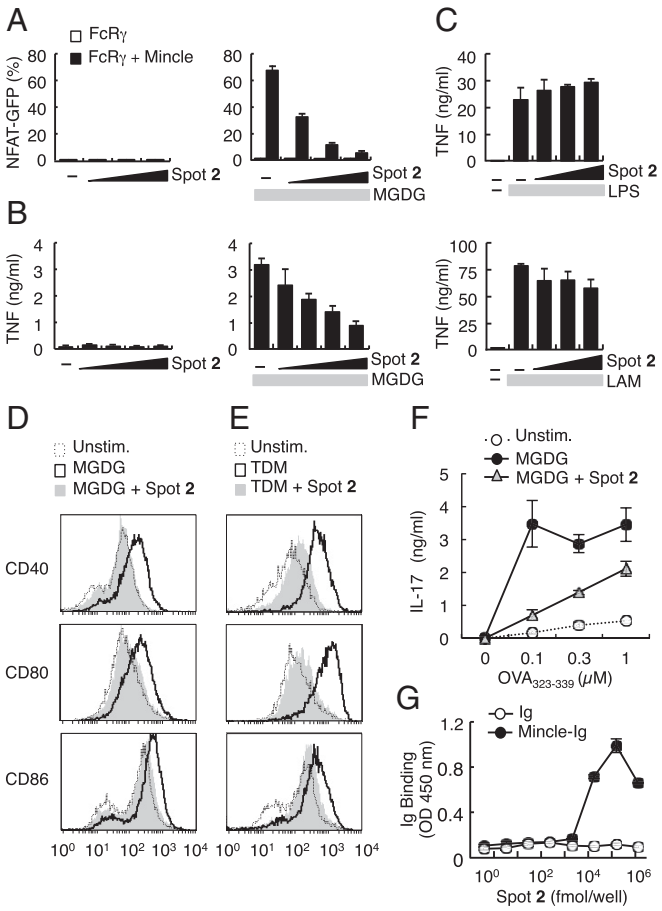

Fig. 6. Identification of a GAS glycolipid that interferes with Mincle-mediated signaling. (*A*) Reporter cells expressing FcRγ only or Mincle + FcRγ were stimulated with the indicated concentrations (0.3, 1, and 3 μg per well) of plate-coated purified Spot **2** in the absence (*Left*) or in the presence (*Right*) of purified MGDG (0.3 μg per well) for 16 h. Induction of NFAT-GFP was analyzed by flow cytometry. (*B*) BMDCs from WT mice were stimulated with indicated concentrations (0.03, 0.1, 0.3, and 1 μg per well) of plate-coated purified Spot **2** for 48 h. The concentration of TNF was determined by ELISA (*Left*). BMDCs from WT mice were stimulated with indicated concentrations (0.03, 0.1, 0.3, and 1 μg per well) of plate-coated purified Spot **2** in the presence of purified MGDG (0.3 μg per well) for 24 h. The concentration of TNF was determined by ELISA (*Right*). (*C*) Effect of Spot **2** on LPS (*Upper*) or LAM (*Lower*)-induced TNF production in BMDCs. (*D* and *E*) BMDCs from WT mice were stimulated with plate-coated (*D*) purified MGDG (30 μg per well) or (*E*) TDM (100 ng per well) in the presence of Spot **2** (30 μg per well) for 48 h. The surface expressions of CD40, CD80, and CD86 were analyzed by flow cytometry. (*F*) BMDCs from WT or Mincle$^{-/-}$ mice were pulsed with $OVA_{323–339}$ peptide and cocultured with $CD4^+$ OT-II T cells for 4 d in the presence of plate-coated purified MGDG (3 μg per well) or plate-coated purified MGDG (3 μg per well) and Spot **2** (3 μg per well). The concentrations of IL-17 secreted into the supernatant were determined by ELISA. (*G*) Ig or Mincle-Ig were incubated with the indicated concentrations of plate-coated purified Spot **2**. Bound proteins were detected with anti–hIgG-HRP. Data are presented as mean ± SD and are representative of three independent experiments with similar results.

NIH34, and K33 clinical isolates were collected by the Working Group for Beta-hemolytic Streptococci in Japan (71). Stock cultures were maintained in 10% glycerol/PBS or 10% skim milk at −80 °C, and SF370 was routinely cultured at 37 °C in Brain Heart Infusion (BHI) broth for 24 h. The number of viable bacteria was determined by counting colony-forming units (CFUs) after diluting and plating onto BHI agar plates. NIH34, K33, NIH44, and Se235 were cultured in Todd Hewitt broth supplemented with 0.5% yeast extract (THY medium). The growth of NIH34 was turbidimetrically monitored at 600 nm, using a MiniPhoto 518R (Taitec). Cultures were grown to late-log phase (OD_{600} = 0.7 to 0.9) at 37 °C in 5% CO_2, pelleted by centrifugation, washed twice with sterile PBS, and suspended in sterile PBS.

Reagents. TDM (T3034), LTA (L3140), and LPS (L4516) were purchased from Merck. Lipoarabinomannan (LAM; 02449-61) was from Nacalai Tesque. Pam3CSK4 (Pam3; tlrl-pms) was from InvivoGen. $OVA_{323–339}$ peptide was obtained from ABGENT. ELISA kits for TNF (558534), IL-6 (555240), and IFNγ (551866) were from BD Bioscience; CXCL10/IP-10/CRG-2 (DY466), CXCL1/KC (DY453-05), MIP-2 (DY452), and IL-17 (DY421) were from R&D Systems; and human IL-8 (88-8086-22) was from eBioscience. Th1/Th2 10 plex FlowCytomix (BMS820FF), MCP-1 (BMS86005FF), IP-10 (BMS86018FF), and CXCL1/KC (BMS86019FF) were from eBioscience. Anti-CD80 (16-10A1) and CD86 (GL-1) antibodies (Abs) were from BioLegend. Anti-CD40 (3/23) antibody (Ab) was from BD Bioscience. Anti-human IgG (H+L) Ab was from Jackson ImmunoResearch. Anti-NOS2 (CXNFT) Ab was from eBioscience. H_2DCFDA was from Molecular Probes. Anti-mouse Mincle Ab (1B6) was described previously (72).

Cells. The 2B4-NFAT-GFP reporter cells expressing various receptors were prepared as previously described (37). BMDCs and human monocyte-derived dendritic cells were also generated as previously described (27, 73). Human embryonic kidney (HEK293) cells expressing secreted alkaline phosphatase (SEAP) under the control of an NF-κB response element were purchased from InvivoGen. The collection and use of human peripheral blood mononuclear cells under written informed consent obtained from all donors were approved by the institutional review boards of Research Institute for Microbial Diseases, Osaka University.

Transcriptome Analysis. Buffy coats were obtained from the Australian Red Cross Blood Service (University of Queensland ethics number HREC2011000232), and $CD14^+$ monocytes, isolated from three donors as previously described (74), were immediately stimulated with GAS strain 5448; or *C. albicans* strain 3630, a clinical isolate obtained from the Australian Medical Mycology Reference Laboratory or *S. typhimurium*. LPS (Invivogen) was used at 10 ng/mL. All pathogens were heat-killed and used at multiplicity of infection (MOI) 10, for 2 h at 37 °C in serum-free RPMI 1640 medium. Cell lysates were collected for RNA (miRNeasy kit; Qiagen). CAGE sequencing was generated as part of the Functional Annotation of Mammalian Genomes 5 (FANTOM5) consortium (32), and primary data are available from the FANTOM5 database (33). For the data described here, Relative log expression normalized expression data (75) were filtered to include only those tags that mapped to an Entrez or HUGO Gene Nomenclature Committee (HGNC) identifier. Multimapped CAGE tags were excluded.

To be considered as input for differential expression analysis, a CAGE tag was required to be expressed at greater than 1 tags per million (TPM) in all donors of a treatment condition, and have a mean expression level greater than in the control condition (i.e., up-regulated), or be expressed at greater than 1 TPM in all donors of the control condition and have a mean expression level greater than in the treatment condition (i.e., down-regulated). Differential expression was assessed by the Rank Product method (76), using the "RankProd" package in R. One thousand permutations were conducted per comparison. Statistically significant differential expression was defined as CAGE tags having a percentage of false prediction value of less than 0.05 and a raw fold change of greater than 1.5-fold. Hypergeometric Optimization of Motif EnRichment (77) was used to analyze enrichment of transcription factor binding sites in the region 500 nucleotides upstream and downstream of the center of a CAGE peak. Enrichment was assessed against a background of all CAGE tags (±500 nucleotides) expressed above 1 TPM in all three Mock donors. Where genomic regions overlapped or book-ended on the same strand, they were merged into a single region using bedtools. Principal component analysis was conducted in R (version 3.2.1) on all expressed TSSs using the "plotPCA" function within the "affycoretools" package. Functional enrichment was conducted using the Protein Analysis Through Evolutionary Relationships (PANTHER) tool (78) interface with Reactome and Gene Ontology (GO).

Lipid Extraction and Purification. GAS was washed with distilled deionized H_2O and then partitioned by C:M:W (8:4:3; vol/vol/vol) into lower organic phase (C:M) and upper aqueous phase (M:W). Lower organic phase was filtered and further fractionated by HPTLC. Each fraction including MGDG and DGDG was developed using the developing solvent C:M:W (85:15:1; vol/vol/vol) and C:M:W (65:25:4; vol/vol/vol), respectively, and collected from the HPTLC plate and dissolved in C:M (2:1; vol/vol).

Synthesis of DGDG. Synthetic DGDG was chemically prepared via 17 reaction steps starting from D-glucose. First, D-glucose was converted into the glucosyl trichloroacetimidate as the glycosyl donor, which possessed two benzyl groups (at C4 and C6 positions) and the 1,1,3,3-tetraisopropyldisiloxanylidene

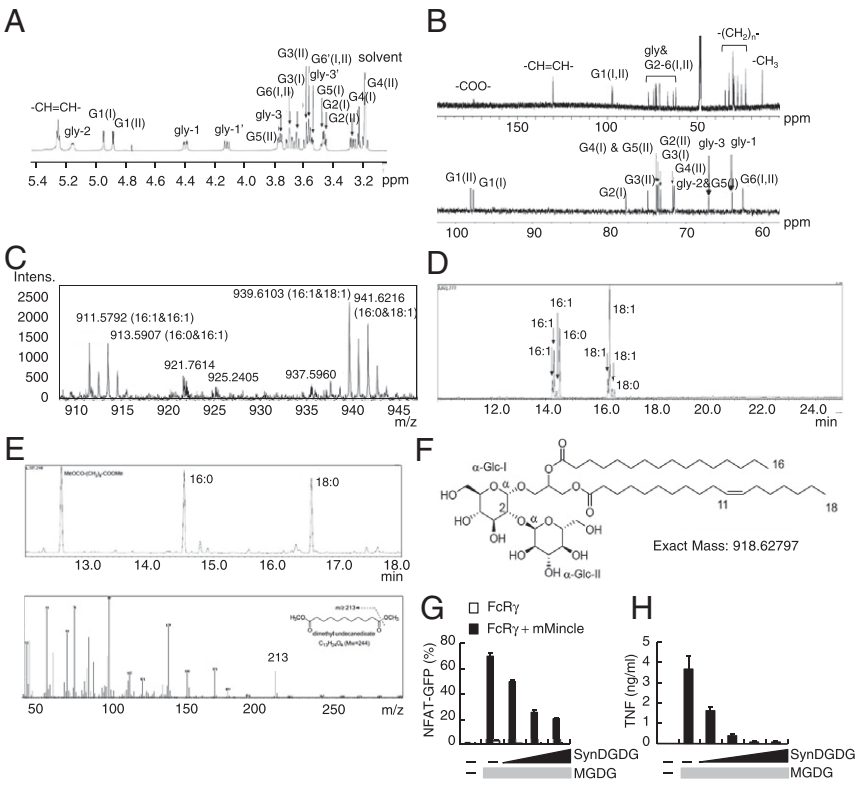

Fig. 7. Chemical identification of Spot 2 as DGDG. The (*A*) ^{1}H-NMR spectrum, (*B*) ^{13}C-NMR spectrum, and (*C*) ESI-TOF-MS spectrum of purified lipids Spot **2**. ESI-TOF-MS data of Spot **2**: *m/z* = 911.5792 $[M+Na]^+$ (calculated for $C_{47}H_{84}NaO_{15}$ Δmmu = −9.0), 913.5907 $[M+Na]^+$ (calculated. for $C_{47}H_{86}NaO_{15}$ Δmmu = −4.8), 939.6103 $[M+Na]^+$ (calculated for $C_{49}H_{88}NaO_{15}$ Δmmu = −8.8), and 941.6216 $[M+Na]^+$ (calculated for $C_{49}H_{90}NaO_{15}$ Δmmu = −4.4). (*D*) GC-MS chromatogram of FAMEs prepared by the methanolysis of Spot **2**: methyl hexadecenoate (16:1), tR [min] = 14.2(7.2%), *m/z* = 268 (M^+); methyl hexadecenoate (16:1), tR [min] = 14.3(17.9%), *m/z* = 268 (M^+); methyl hexadecenoate (16:1), tR [min] = 14.4 (2.7%), *m/z* = 268 (M^+); methyl hexadecanoate (16:0), tR [min] = 14.5(19.0%), *m/z* = 270 (M^+); methyl octadecenoate (18:1), tR [min] = 16.3(7.0%), *m/z* = 296 (M^+); methyl octadecenoate (18:1), tR [min] = 16.4(41.5%), *m/z* = 296 (M^+); methyl octadecenoate (18:1), tR [min] = 16.5(2.8%), *m/z* = 296 (M^+); and methyl octadecenoate (18:0), tR [min] = 16.6(1.9%), *m/z* = 298 (M^+). (*E*) FAMEs of Spot **2** after $RuCl_3$/$NaIO_4$ oxidation: dimethyl undecanedioate (11:0), tR [min] = 12.6, *m/z* = 213 (M^+−31). (*F*) Chemical structure of DGDG (Spot **2**) from GAS. (*G* and *H*) Effect of synthetic DGDG (SynDGDG) on MGDG-induced activation of (*G*) Mincle reporter cells and (*H*) BMDCs. SynDGDG (*G*: 0.3, 1, 3 μg per well), (*H*: 0.03, 0.1, 0.3, 1 μg per well) was coated together with MGDG (0.3 μg per well).

group (bridged between C2 and C3) as protecting groups. The glucosyl donor was next coupled with (*S*)-(+)-1,2-isopropylideneglycerol in the presence of trimethylsilyl triflate in CH_2Cl_2 at –80 °C, affording the glucosyl glycerol derivative in 61% yield (α/β ratio = 1:3). Subsequent hydrogenolysis of the isolated β-glucosyl glycerol provided the corresponding glucosyl glycerol acceptor, which was then subjected to the second glycosylation with the

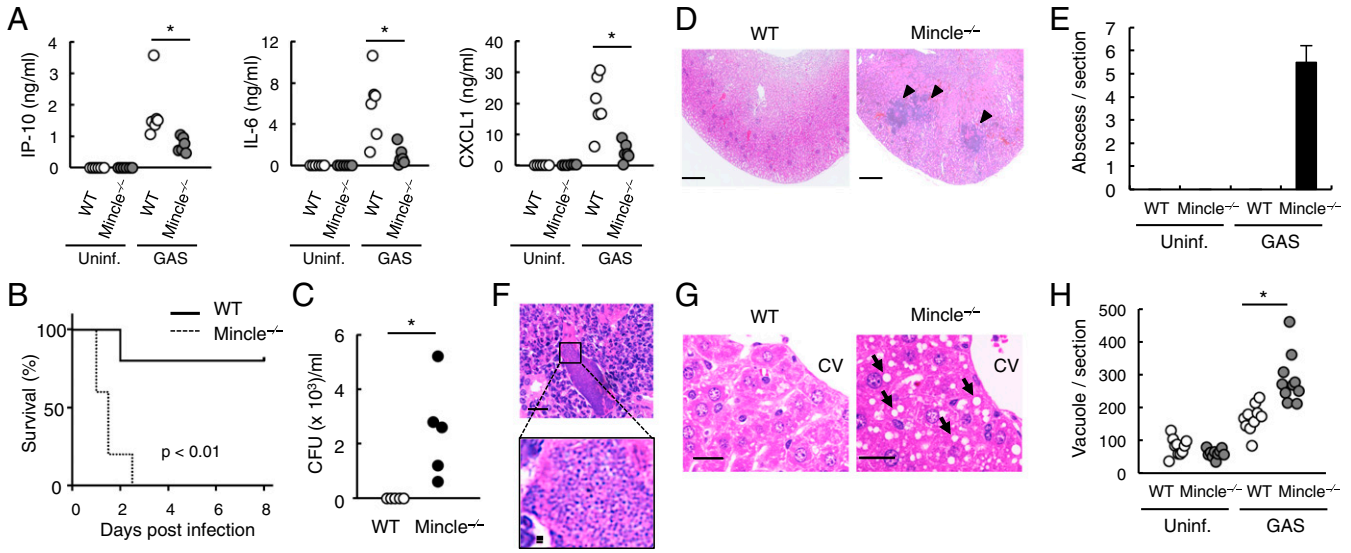

Fig. 8. Critical role of Mincle in GAS infection. (*A*) The concentrations of IP-10, IL-6, and CXCL1 in the serum from uninfected or infected mice 3 h after i.p. infection with 1.5×10^8 CFUs of NIH34. The concentrations of cytokines and chemokines were determined by FlowCytomix and ELISA. **P* < 0.05. (*B*) Survival curves of WT (solid line) and Mincle$^{-/-}$ (dotted line) mice after i.p. infection with 2.3×10^7 CFU of NIH34. Groups of 5 Mincle$^{-/-}$ or WT mice were infected, and survival was monitored over 8 d. Comparison of survival curves was performed using the log-rank test. Data are representative of two independent experiments with similar results. (*C*) Kinetics of GAS bacterial growth in the blood of WT (*n* = 5) or Mincle$^{-/-}$ (*n* = 5) mice at 48 h after i.p. infection with 1.4×10^7 CFU of NIH34. The number of bacteria was compared by the Mann–Whitney *U* test. **P* < 0.05. (*D*) Histopathological changes in the kidney of WT (*Left*) or Mincle$^{-/-}$ (*Right*) mice infected with 1.4×10^7 CFU of NIH34. Tissues were collected at 48 h after the i.p. injection of GAS and stained with hematoxylin and eosin. The black arrowheads indicate abscesses infiltrated with inflammatory cells. (Scale bar: 500 μm.) (*E*) Quantification of abscesses in the kidney sections of WT and Mincle$^{-/-}$ mice. (*F*) The clusters of bacteria in the kidney. (Scale bar: 20 μm in *Upper* and 2 μm in *Lower*.) (*G*) Histopathological changes in the liver of WT (*Left*) or Mincle$^{-/-}$ (*Right*) mice infected with 1.4×10^7 CFU of NIH34. Tissues were collected at 48 h after i.p. injection of GAS and stained with hematoxylin and eosin. The black arrows indicate hepatocellular vacuolation. (Scale bar: 20 μm.) CV, centrilobular vein. (*H*) Quantification of hepatocellular vacuolation in the liver sections of WT and Mincle$^{-/-}$ mice. **P* < 0.05.

above-mentioned glucosyl donor. The glycosylation gave the gentiobiosyl glycerol derivative in 67% yield along with good β-stereoselectivity (α/β ratio = 1:19). Subsequent hydrolysis with 85% aqueous acetic acid removed the isopropylidene group on the glycerol moiety. Then, both regioselective acylation of the primary alcohol with heptadecanoic acid and subsequent acylation of the secondary alcohol on the glycerol moiety with pentadecanoic acid were achieved by the action of N,N′-dicyclohexylcarbodiimide and 4-(dimethylamino) pyridine in CH_2Cl_2 at −5 °C, affording the desired DGDG framework. Finally, global deprotection furnished the targeted synthetic DGDG.

In Vitro Infection. BMDCs were plated in a 12-well plate and infected with the GAS strains and incubated for 2 h in antibiotic-free medium at 37 °C in 5% CO_2. BMDCs were washed with PBS to remove unbound bacteria and further incubated with complete medium in the presence of streptomycin (100 μg/mL) and penicillin (57.6 μg/mL) at 37 °C in 5% CO_2 for 16 h.

In Vitro Stimulation. GAS lipid extracts and TDM were dissolved in C:M (2:1; vol/vol) or methanol, diluted with isopropanol, and added on wells, followed by evaporation of the solvent as previously described (25). GAS hydrophilic extracts were dissolved in distilled deionized H_2O and added to the culture medium. The 2B4-NFAT-GFP reporter cells were stimulated for 16 h, and the activation of NFAT-GFP was monitored by FACSCalibur flow cytometry (BD Biosciences). BMDCs (1×10^5 cells per well) were stimulated for 2 d, and the culture supernatants were collected to determine the concentrations of each cytokine by ELISA. Activation of BMDCs was evaluated using surface staining of the costimulatory molecules such as CD40, CD80, and CD86 by flow cytometry. For iNOS measurement, BMDCs were stimulated for 2 h and further incubated for 16 h with 2 μM Brefeldin A. Intracellular iNOS was detected with anti-NOS2 Ab by flow cytometry. For ROS measurement, BMDCs were stimulated for 24 h and further incubated with 10 μM H_2DCFDA at 37 °C for 30 min followed by flow cytometry analysis.

In Vitro Mincle Binding Assay. Mincle-Ig fusion proteins were prepared as described previously (72). In brief, the C terminus of the extracellular domain of mouse Mincle (a.a. 46 to 214) was fused to the N terminus of hIgG1 Fc region. Then 10 μg/mL of hIgG1-Fc (Ig) or Mincle-Ig in binding buffer (20 mM Tris·HCl, 150 mM NaCl, 1 mM $CaCl_2$, 2 mM $MgCl_2$, pH 7.0) was incubated with plate-coated lipids. Bound protein was detected with anti−hIgG-HRP followed by the addition of colorimetric substrate. Peroxidase activity was measured spectrophotometerically. For Mincle-Ig binding to intact GAS, live GAS was incubated with Mincle-Ig (1 μg/mL) for 1 h at 4 °C. Bound proteins were detected with anti−hIgG-Alexa 488 by flow cytometry.

ESI-TOF-MS and NMR. ESI-TOF-MS was measured with a Bruker microTOF mass spectrometer in the positive ESI mode (Bruker Daltonics). For NMR experiments, ^{1}H- and ^{13}C-NMR spectra were recorded on an Agilent INOVA 600 spectrometer. The operating conditions were as follows: ^{1}H: 600 MHz, 298 K, $CDCl_3/CD_3OD/D_2O$ (60:35:5; vol/vol/vol); ^{13}C: 125 MHz, 298 K, $CDCl_3/CD_3OD/D_2O$ (60:35:5; vol/vol/vol). The ^{1}H- and ^{13}C chemical shifts were assigned by 2D-NMR (COSY, TOCSY, HSQC, HMBC) experiments. The ^{1}H chemical shift was referenced to trimethylsilane (δ_H 0), and the ^{13}C chemical shift was referenced to CD_3OD (δ_C 49.0).

GC-MS Analysis of MGDG and DGDG. For methanolysis, MGDG or DGDG (each *ca*. 100 μg) was heated with 10% HCl/MeOH (100 μL) in a sealed tube at 90 °C for 3 h. The reaction mixture was diluted with MeOH (0.4 mL) and extracted with *n*-hexane (200 μL × 2), and the *n*-hexane extract was concentrated in vacuo to give a mixture of FAMEs. The FAMEs were dissolved in acetone and subjected to GC-MS [Shimadzu QP-2010SE with INERTCAP 5MS/SIL (0.25 mm i.d., ×30 m); GL Science Inc.; column temperature 100 °C to 280 °C; rate of temperature increase: 10 °C/min]. Part of the FAMEs sample was dissolved in $CCl_4/CH_3CN/H_2O$ (1/1/1, each 50 μL), with added $RuCl_3/NaIO_4$ (1/1, each 50 μg), and vigorously stirred at room temperature. After 1 h, the reaction mixture was diluted with H_2O (100 μL) and extracted with Et_2O (100 μL). The Et_2O was dried with N_2 gas and incubated in 20% MeOH/benzene (50 μL) and trimethylsilyl-CH_2CN (50 μL) at 50 °C for 30 min. The reaction mixture was dried with N_2 gas, and was diluted with *n*-hexane and subjected to GC-MS. The position of the double bond in major unsaturated FAME (16:1) was determined by the identification of dimethyl undecanedioate [MeOCO-$(CH_2)_9$-COOMe] using $RuCl_3/NaIO_4$ oxidation followed by GC-MS analysis.

CD4$^+$ T-Cell Responses. BMDCs from WT or Mincle-deficient mice were left untreated or stimulated with indicated amounts of plate-coated purified MGDG and TDM in the presence of $OVA_{323–339}$ peptide. CD4$^+$ T cells from OT-II Tg mice were purified with anti−CD4-conjugated magnetic beads (Miltenyi Biotec) and cocultured with OVA-pulsed BMDCs in 96-well plates. On day 4, the supernatants were collected, and the concentrations of IFNγ and IL-17 were determined by ELISA.

GAS Infection. GAS strains were grown to late-log phase (OD_{600} = 0.7 to 0.9), resuspended in PBS and injected intraperitoneally, as previously described (57), into 5- to 6-wk-old Mincle-deficient or C57BL/6 male mice. Survival curves were compared using a log-rank test in GraphPad Prism 6. For measurement of bacterial load, at 48 h postinfection, 20 μL of peripheral blood was removed from the tail vein by phlebotomy. The blood was diluted at 1:10 to 1:1,000 with PBS and spread on a Columbia agar plate containing 5% sheep blood (BD). To determine the number of CFUs in peripheral blood, the plates were incubated for 20 h at 37 °C in 5% CO_2, and the colonies were counted. The number of CFUs was compared statistically using the Mann–Whitney *U* test. The concentrations of cytokines and chemokines in plasma were determined by FlowCytomix (eBioscience) according to the manufacturer's instructions.

Histology Analysis. The tissues of kidney, liver, and lung from GAS-infected mice were fixed in 10% formalin/PBS. The paraffin-embedded sections were stained with hematoxylin and eosin. The semiquantitative analysis included measurement of abscesses in the kidney, and hepatocellular vacuoles in the liver using BZ-X analyzer (Keyence).

Statistics. An unpaired two-tailed Student's *t* test was used for all statistical analyses unless otherwise specified.

ACKNOWLEDGMENTS. We thank T. Hara for supervision; M. Kurata, S. Iwai, X. Lu, and K. Motomura for technical support; M. Tanaka, Y. Baba, K. Kaseda, and M. Ikawa for embryonic engineering; and the Cooperative Research Project Program of the Medical Institute of Bioregulation, Kyushu University. This research was supported by Japan Society for the Promotion of Science (JSPS) KAKENHI Grants JP26293099 (to S.Y.), JP26110009 (to S.Y.), and JP16K09952 (to T. Matsumura); Japan Agency for Medical Research and Development (AMED) under Grants JP17gm0910010 (to S.Y.), JP17ak0101070 (to S.Y.), JP18fk0108075 (to S.Y.), and JP18fk0108044 (to T. Ikebe and T. Matsumura); Vidi Grant 91713303 from the Netherlands Organization for Scientific Research (to N.M.v.S.); National Health and Medical Research Council (NHMRC) Grants APP1041294 and APP1057846 (to M.J.W. and C.A.W.); and the Australian Research Council Grant SRI110001002 (to C.A.W.). S.Y. acknowledges funding from Takeda Science Foundation. B.L. acknowledges funding from the Niedersachsen-Research Network on Neuroinfectiology.

1. Johansson L, Thulin P, Low DE, Norrby-Teglund A (2010) Getting under the skin: The immunopathogenesis of *Streptococcus pyogenes* deep tissue infections. *Clin Infect Dis* 51:58–65.
2. Woldu B, Bloomfield GS (2016) Rheumatic heart disease in the twenty-first century. *Curr Cardiol Rep* 18:96.
3. Walker MJ, et al. (2014) Disease manifestations and pathogenic mechanisms of group A *Streptococcus*. *Clin Microbiol Rev* 27:264–301.
4. Medina E, Goldmann O, Rohde M, Lengeling A, Chhatwal GS (2001) Genetic control of susceptibility to group A streptococcal infection in mice. *J Infect Dis* 184:846–852, and erratum (2001) 184:1368.
5. Goldmann O, Rohde M, Chhatwal GS, Medina E (2004) Role of macrophages in host resistance to group A Streptococci. *Infect Immun* 72:2956–2963.
6. Fieber C, Kovarik P (2014) Responses of innate immune cells to group A *Streptococcus*. *Front Cell Infect Microbiol* 4:140.
7. Mishalian I, et al. (2011) Recruited macrophages control dissemination of group A *Streptococcus* from infected soft tissues. *J Immunol* 187:6022–6031.
8. Hidalgo-Grass C, et al. (2006) A streptococcal protease that degrades CXC chemokines and impairs bacterial clearance from infected tissues. *EMBO J* 25:4628–4637.
9. Loof TG, Goldmann O, Medina E (2008) Immune recognition of *Streptococcus pyogenes* by dendritic cells. *Infect Immun* 76:2785–2792.
10. Gratz N, et al. (2008) Group A Streptococcus activates type I interferon production and MyD88-dependent signaling without involvement of TLR2, TLR4, and TLR9. *J Biol Chem* 283:19879–19887.
11. Harder J, et al. (2009) Activation of the Nlrp3 inflammasome by *Streptococcus pyogenes* requires streptolysin O and NF-kappa B activation but proceeds independently of TLR signaling and P2X7 receptor. *J Immunol* 183:5823–5829.
12. Loof TG, Goldmann O, Gessner A, Herwald H, Medina E (2010) Aberrant inflammatory response to *Streptococcus pyogenes* in mice lacking myeloid differentiation factor 88. *Am J Pathol* 176:754–763.
13. Schwandner R, Dziarski R, Wesche H, Rothe M, Kirschning CJ (1999) Peptidoglycan- and lipoteichoic acid-induced cell activation is mediated by toll-like receptor 2. *J Biol Chem* 274:17406–17409.
14. Oldenburg M, et al. (2012) TLR13 recognizes bacterial 23S rRNA devoid of erythromycin resistance-forming modification. *Science* 337:1111–1115.

15. Hidmark A, von Saint Paul A, Dalpke AH (2012) Cutting edge: TLR13 is a receptor for bacterial RNA. *J Immunol* 189:2717–2721.
16. Fieber C, et al. (2015) Innate immune response to *Streptococcus pyogenes* depends on the combined activation of TLR13 and TLR2. *PLoS One* 10:e0119727.
17. Zinkernagel AS, et al. (2012) Importance of toll-like receptor 9 in host defense against M1T1 group A *Streptococcus* infections. *J Innate Immun* 4:213–218.
18. Fernandez I, et al. (2014) Invasive group A *Streptococcus* disease in French-Canadian children is not associated with a defect in MyD88/IRAK4-pathway. *Allergy Asthma Clin Immunol* 10:9.
19. Valderrama JA, et al. (2017) Group A streptococcal M protein activates the NLRP3 inflammasome. *Nat Microbiol* 2:1425–1434.
20. Geijtenbeek TB, Gringhuis SI (2016) C-type lectin receptors in the control of T helper cell differentiation. *Nat Rev Immunol* 16:433–448.
21. Hoving JC, Wilson GJ, Brown GD (2014) Signalling C-type lectin receptors, microbial recognition and immunity. *Cell Microbiol* 16:185–194.
22. Ostrop J, Lang R (2017) Contact, collaboration, and conflict: Signal integration of Syk-coupled C-type lectin receptors. *J Immunol* 198:1403–1414.
23. Hara H, et al. (2007) The adaptor protein CARD9 is essential for the activation of myeloid cells through ITAM-associated and toll-like receptors. *Nat Immunol* 8:619–629.
24. Wu W, Hsu YM, Bi L, Songyang Z, Lin X (2009) CARD9 facilitates microbe-elicited production of reactive oxygen species by regulating the LyGDI-Rac1 complex. *Nat Immunol* 10:1208–1214.
25. Ishikawa E, et al. (2009) Direct recognition of the mycobacterial glycolipid, trehalose dimycolate, by C-type lectin Mincle. *J Exp Med* 206:2879–2888.
26. Ishikawa T, et al. (2013) Identification of distinct ligands for the C-type lectin receptors Mincle and Dectin-2 in the pathogenic fungus *Malassezia*. *Cell Host Microbe* 13: 477–488.
27. Miyake Y, et al. (2013) C-type lectin MCL is an FcRγ-coupled receptor that mediates the adjuvanticity of mycobacterial cord factor. *Immunity* 38:1050–1062.
28. Toyonaga K, et al. (2016) C-type lectin receptor DCAR recognizes mycobacterial phosphatidyl-inositol mannosides to promote a Th1 response during infection. *Immunity* 45:1245–1257.
29. Yonekawa A, et al. (2014) Dectin-2 is a direct receptor for mannose-capped lipoarabinomannan of mycobacteria. *Immunity* 41:402–413.
30. Behler-Janbeck F, et al. (2016) C-type lectin Mincle recognizes glucosyl-diacylglycerol of *Streptococcus pneumonia*e and plays a protective role in pneumococcal pneumonia. *PLoS Pathog* 12:e1006038.
31. Lu X, Nagata M, Yamasaki S (2018) Mincle: 20 years of a versatile sensor of insults. *Int Immunol* 30:233–239.
32. Forrest AR, et al.; FANTOM Consortium and the RIKEN PMI and CLST (DGT) (2014) A promoter-level mammalian expression atlas. *Nature* 507:462–470.
33. Lizio M, et al.; FANTOM consortium (2015) Gateways to the FANTOM5 promoter level mammalian expression atlas. *Genome Biol* 16:22.
34. Gross O, et al. (2006) Card9 controls a non-TLR signalling pathway for innate anti-fungal immunity. *Nature* 442:651–656.
35. Wells CA, et al. (2008) The macrophage-inducible C-type lectin, Mincle, is an essential component of the innate immune response to *Candida albicans*. *J Immunol* 180:7404–7413.
36. Brown GD (2006) Dectin-1: A signalling non-TLR pattern-recognition receptor. *Nat Rev Immunol* 6:33–43.
37. Takano T, et al. (2017) Dectin-1 intracellular domain determines species-specific ligand spectrum by modulating receptor sensitivity. *J Biol Chem* 292:16933–16941.
38. Feinberg H, et al. (2013) Mechanism for recognition of an unusual mycobacterial glycolipid by the macrophage receptor Mincle. *J Biol Chem* 288:28457–28465.
39. Furukawa A, et al. (2013) Structural analysis for glycolipid recognition by the C-type lectins Mincle and MCL. *Proc Natl Acad Sci USA* 110:17438–17443.
40. Bogdan C (2001) Nitric oxide and the immune response. *Nat Immunol* 2:907–916.
41. Ito C, et al. (2013) Endogenous nitrated nucleotide is a key mediator of autophagy and innate defense against bacteria. *Mol Cell* 52:794–804.
42. Goldmann O, et al. (2007) Transcriptome analysis of murine macrophages in response to infection with *Streptococcus pyogenes* reveals an unusual activation program. *Infect Immun* 75:4148–4157.
43. Schneewind O, Missiakas D (2014) Lipoteichoic acids, phosphate-containing polymers in the envelope of gram-positive bacteria. *J Bacteriol* 196:1133–1142.
44. Ray A, Cot M, Puzo G, Gilleron M, Nigou J (2013) Bacterial cell wall macroamphiphiles: Pathogen-/microbe-associated molecular patterns detected by mammalian innate immune system. *Biochimie* 95:33–42.
45. Kerscher B, et al. (2016) Signalling through MyD88 drives surface expression of the mycobacterial receptors MCL (Clecsf8, Clec4d) and Mincle (Clec4e) following microbial stimulation. *Microbes Infect* 18:505–509.
46. Schoenen H, et al. (2014) Differential control of Mincle-dependent cord factor recognition and macrophage responses by the transcription factors C/EBPβ and HIF1α. *J Immunol* 193:3664–3675.
47. LaRock CN, et al. (2016) IL-1beta is an innate immune sensor of microbial proteolysis. *Sci Immunol* 1:eaah3539.
48. Castiglia V, et al. (2016) Type I interferon signaling prevents IL-1β-driven lethal systemic hyperinflammation during invasive bacterial infection of soft tissue. *Cell Host Microbe* 19:375–387.
49. Lin AE, et al. (2015) A group A Streptococcus ADP-ribosyltransferase toxin stimulates a protective interleukin 1β-dependent macrophage immune response. *MBio* 6:e00133.
50. Schweneker K, et al. (2013) The mycobacterial cord factor adjuvant analogue trehalose-6,6′-dibehenate (TDB) activates the Nlrp3 inflammasome. *Immunobiology* 218:664–673.
51. Gross O, et al. (2009) Syk kinase signalling couples to the Nlrp3 inflammasome for anti-fungal host defence. *Nature* 459:433–436.
52. Matsumoto M, et al. (1999) A novel LPS-inducible C-type lectin is a transcriptional target of NF-IL6 in macrophages. *J Immunol* 163:5039–5048.
53. Yamasaki S, et al. (2009) C-type lectin Mincle is an activating receptor for pathogenic fungus, *Malassezia*. *Proc Natl Acad Sci USA* 106:1897–1902.
54. Lee WB, et al. (2012) Neutrophils promote mycobacterial trehalose dimycolate-induced lung inflammation via the Mincle pathway. *PLoS Pathog* 8:e1002614.
55. Behler F, et al. (2012) Role of Mincle in alveolar macrophage-dependent innate immunity against mycobacterial infections in mice. *J Immunol* 189:3121–3129.
56. Loof TG, Rohde M, Chhatwal GS, Jung S, Medina E (2007) The contribution of dendritic cells to host defenses against *Streptococcus pyogenes*. *J Infect Dis* 196:1794–1803.
57. Matsumura T, et al. (2012) Interferon-γ-producing immature myeloid cells confer protection against severe invasive group A *Streptococcus* infections. *Nat Commun* 3:678.
58. Shaw N (1970) Bacterial glycolipids. *Bacteriol Rev* 34:365–377.
59. Doran KS, et al. (2005) Blood-brain barrier invasion by group B *Streptococcus* depends upon proper cell-surface anchoring of lipoteichoic acid. *J Clin Invest* 115: 2499–2507.
60. Huang H, et al. (2012) Relative contributions of dectin-1 and complement to immune responses to particulate β-glucans. *J Immunol* 189:312–317.
61. Maneu V, et al. (2011) Dectin-1 mediates in vitro phagocytosis of *Candida albicans* yeast cells by retinal microglia. *FEMS Immunol Med Microbiol* 63:148–150.
62. Ofek I, Simpson WA, Beachey EH (1982) Formation of molecular complexes between a structurally defined M protein and acylated or deacylated lipoteichoic acid of *Streptococcus pyogenes*. *J Bacteriol* 149:426–433.
63. Wang B, et al. (2010) Induction of TGF-beta1 and TGF-beta1-dependent predominant Th17 differentiation by group A streptococcal infection. *Proc Natl Acad Sci USA* 107: 5937–5942.
64. Linehan JL, et al. (2015) Generation of Th17 cells in response to intranasal infection requires TGF-β1 from dendritic cells and IL-6 from CD301b+ dendritic cells. *Proc Natl Acad Sci USA* 112:12782–12787.
65. Sanchez M, et al. (2017) O-acetylation of peptidoglycan limits helper T cell priming and permits *Staphylococcus aureus* reinfection. *Cell Host Microbe* 22:543–551.e4.
66. Khader SA, et al. (2007) IL-23 and IL-17 in the establishment of protective pulmonary CD4+ T cell responses after vaccination and during Mycobacterium tuberculosis challenge. *Nat Immunol* 8:369–377.
67. Shenderov K, et al. (2013) Cord factor and peptidoglycan recapitulate the Th17-promoting adjuvant activity of mycobacteria through Mincle/CARD9 signaling and the inflammasome. *J Immunol* 190:5722–5730.
68. Mortensen R, et al. (2017) Local Th17/IgA immunity correlate with protection against intranasal infection with *Streptococcus pyogenes*. *PLoS One* 12:e0175707.
69. Cunningham MW (2012) Streptococcus and rheumatic fever. *Curr Opin Rheumatol* 24: 408–416.
70. Hoy WE, et al. (2012) Post-streptococcal glomerulonephritis is a strong risk factor for chronic kidney disease in later life. *Kidney Int* 81:1026–1032.
71. Ikebe T, et al. (2010) Highly frequent mutations in negative regulators of multiple virulence genes in group A streptococcal toxic shock syndrome isolates. *PLoS Pathog* 6:e1000832.
72. Yamasaki S, et al. (2008) Mincle is an ITAM-coupled activating receptor that senses damaged cells. *Nat Immunol* 9:1179–1188.
73. Kiyotake R, et al. (2015) Human Mincle binds to cholesterol crystals and triggers innate immune responses. *J Biol Chem* 290:25322–25332.
74. Vijayan D, Radford KJ, Beckhouse AG, Ashman RB, Wells CA (2012) Mincle polarizes human monocyte and neutrophil responses to *Candida albicans*. *Immunol Cell Biol* 90: 889–895.
75. Robinson MD, McCarthy DJ, Smyth GK (2010) edgeR: A bioconductor package for differential expression analysis of digital gene expression data. *Bioinformatics* 26:139–140.
76. Breitling R, Armengaud P, Amtmann A, Herzyk P (2004) Rank products: A simple, yet powerful, new method to detect differentially regulated genes in replicated microarray experiments. *FEBS Lett* 573:83–92.
77. Heinz S, et al. (2010) Simple combinations of lineage-determining transcription factors prime cis-regulatory elements required for macrophage and B cell identities. *Mol Cell* 38:576–589.
78. Mi H, Muruganujan A, Casagrande JT, Thomas PD (2013) Large-scale gene function analysis with the PANTHER classification system. *Nat Protoc* 8:1551–1566.